Article

SHM Structural Health Monitoring

Structural Health Monitoring
0(0) 1–13

DOI: 10.1177/1475921712451954
shm.sagepub.com
SAGE

# Predictive modeling of electromechanical impedance spectroscopy for composite materials

**Matthieu Gresil, Lingyu Yu, Victor Giurgiutiu and Michael Sutton**

**Abstract**

The advancement of composite materials in aircraft structures has led to an increased need for effective structural health monitoring technologies that are able to detect and assess damage present in composite structures. The study presented in this article is interested in understanding self-sensing piezoelectric wafer sensors to conduct electromechanical impedance spectroscopy in glass fiber reinforced polymer composite to perform structural health monitoring. For this objective, multi-physics-based finite element method is used to model the electromechanical behavior of a free piezoelectric wafer active sensor and its interaction with the host structure on which it is bonded. The multi-physics-based modeling permits the input and output variables to be expressed directly in electric terms, while the two-way electromechanical conversion is done internally in the multi-physics-based finite element method formulation. The impedance responses are also studied in conditions when the sensor bonding layer is subject to degradation and when the sensor itself is subjected to breakage, respectively. To reach the goal of using the electromechanical impedance spectroscopy approach to detect damage, several damage models are generated on simplified orthotropic structure and laminated glass fiber reinforced polymer structures. The effects of the modeling are carefully studied through experimental validation. A good match has been observed for low and high frequencies.

**Keywords**

Electromechanical impedance spectroscopy, composite materials, finite element modeling, structural health monitoring, piezoelectric wafer active sensors

## Introduction

Electromechanical impedance spectroscopy (EMIS) using self-sensing piezoelectric wafer active sensors (PWASs) has been shown as an effective structural health monitoring (SHM) technique, and has useful applications in various fields of engineering: mechanical, aerospace, civil, and others.[1] PWAS operates on piezoelectric principles. When bonded onto the structure, the electrical impedance measured at its terminals is coupled with local structural–mechanical impedance such that the mechanical resonance spectrum of the structure is reflected in a virtually identical spectrum of peaks and valleys in the real part of the electro-mechanical (E/M) impedance spectrum. The PWAS–EMIS method utilizes high-frequency excitations, typically higher than 30 kHz and lower than 10 MHz, to monitor changes in the structural–mechanical impedance. The PWASs require very low voltage (~1 V) to produce high-frequency excitation in the structure.

Over the past decade, substantial efforts have been devoted to the analytical and numerical modeling of various aspects of the EMIS method.[2–9] However, the majority of prior studies are focused on fundamental understanding of the sensor–transduction mechanism and sensor–structure interaction. Analytical models are often unsuitable for practical applications because they only consider simple structures such as beams, plates, and shells with easy to simulate boundary conditions. More importantly, most of the previous study is on isotropic (such as metallic) or heterogeneous (such as

Department of Mechanical Engineering, University of South Carolina, Columbia, SC, USA

**Corresponding author:**
Matthieu Gresil, Department of Mechanical Engineering, University of South Carolina, 300 Main Street, Columbia, SC 29208, USA
Email: matthieu@engr.sc.edu

concrete) structures. EMIS applications to orthotropic-laminated composites have also been studied and discussed in the literature to a lesser extent.[10,11] Subsequent developments in various numerical methods, such as the finite element method (FEM), were found to be an ideal alternative.

With the help of powerful commercial software, the FEM modeling and analysis process is becoming increasingly efficient. Various FEM models on PWAS–structure interaction have been proposed since the 1990s. Lalande[3] attempted the dynamic FEM of shell structure using the commercially available software ANSYS. Good correlation was found between the FEM results and results from the impedance based on the analytical model. Lim[4] showed reasonably good comparison of mechanical impedance between the experiment and the FEM-based impedance model for an aluminum beam. At low frequency of excitation, simplification of the PWAS into a force or moment is normally acceptable. However, at high frequency of excitation, such as in the application of the EMIS technique, such simplification could lead to considerable loss in accuracy. Liu and Giurgiutiu[5] compared experimental measurements on a beam structure with the impedance calculated with both a conventional FEM model mechanically coupled to the PWAS and a coupled-field multi-physics-based finite element method (MP-FEM) model in which the PWAS was directly excited electrically. The coupled-field FEM model exhibited closer agreement to the experimental results.

In SHM studies, finite element simulations have shown the ability to model structural defects and damage. Naidu and Soh[6] developed an FEM model of an elastic beam in which damage was introduced by changing the stiffness parameters of selected elements. Natural frequencies of damaged and undamaged beams were calculated and compared. They indicated that the effectiveness of the diagnosis method depends on the location of the PWAS. Among all the preceding efforts, only a limited number of investigations address FEM simulation of both EMIS and structural damage for isotropic material. Modeling of practical structural diagnostic scenarios remains a challenge.

This article presents finite element modeling of PWAS EMIS applications on glass fiber reinforced composite structures. Issues related to energy dissipation in the piezoelectric sensor and host composite structure, as well as its effect on detectability of structural damage are studied using multi-physics-based models. The MP-FEM implementation allows for the consideration of the contributions of the active material, the adhesive bond, and the structural damage. The study shows that sensor position may directly control damage manifestation in EMIS signature; the effect of adhesive bond thickness is comparable in magnitude to the effect of bond stiffness; and the influence of piezoelectric mechanical losses on the impedance signature is different for damaged and undamaged cases.

## EMIS

PWAS can be used as active sensing devices that provide bidirectional energy transduction from the electronics into the structure and also from the structure back into the electronics. PWAS can be used as collocated E/M impedance sensor–actuators that permit effective modal identification in a wide frequency band.[8,12–14] In an embedded sensing system, the PWAS can be embedded into the structures by mounting them directly onto the structure and then leaving them in place to perform their SHM task (such a thing would be unthinkable with conventional ultrasonic transducers, which are bulky, obtrusive, and expensive) (Figure 1).

### *The PWAS electromechanical impedance method*

For a linear piezoelectric material, the relation between the electrical and the mechanical variables can be described by linear relations

$$\begin{bmatrix} S \\ D \end{bmatrix} = \begin{bmatrix} s^E & d_t \\ d & \varepsilon^T \end{bmatrix} \begin{bmatrix} T \\ E \end{bmatrix} \tag{1}$$

where $S$ is the mechanical strain, $T$ is the mechanical stress, $E$ is the electric field, $D$ is the charge density, $s$ is the mechanical compliance, $d$ is the piezoelectric strain constant, and $\varepsilon$ is the permittivity. The superscripts $E$ and $T$ indicate that these quantities are measured with electrodes connected together and zero stress, respectively, and the subscript $t$ indicates transpose. The first equation describes the converse piezoelectric effect and the second describes the direct effect.

The principles of E/M impedance method are illustrated in Figure 2. The drive-point impedance presented by the structure to the active sensor can be expressed as the frequency dependent variable

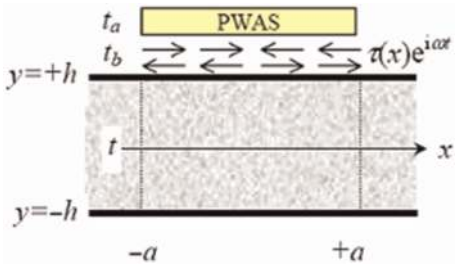


**Figure 1.** Interaction between the PWAS and the structure.
PWAS: piezoelectric wafer active sensor.

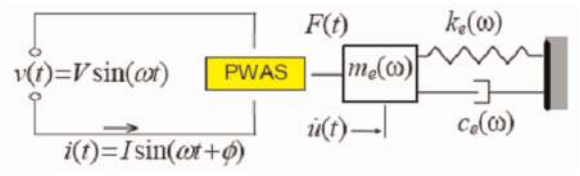


**Figure 2.** E/M coupling between PWAS and structure for an 1D dynamic model.
1D: one-dimensional.

$Z_{str}(\omega) = k_{str}(\omega)/j\omega = k_e(\omega) - \omega_m^2(\omega) + j\omega c_e(\omega)$. Through the mechanical coupling between PWAS and the host structure, on one hand, and through the E/M transduction inside the PWAS, on the other hand, the drive-point structural impedance is reflected directly in the electrical impedance, $Z(\omega)$, at the PWAS terminals

$$Z(\omega) = \left[ j\omega c \left( 1 - \kappa_{31}^2 \frac{\chi(\omega)}{1 + \chi(\omega)} \right) \right]^{-1} \quad (2)$$

where $c$ is the zero-load capacitance of the PWAS and $\kappa_{31}$ is the E/M cross coupling coefficient of the PWAS ($\kappa_{31} = d_{31}/\sqrt{\bar{s}_{11}\bar{\varepsilon}_{33}}$), and $\chi(\omega) = k_{str}/k_{\text{PWAS}}$ with $k_{\text{PWAS}}$ being the static stiffness of the PWAS.

### *PWAS EMIS experimental measurement*

The E/M impedance SHM method is direct and easy to implement, the only required equipment being an electrical impedance analyzer, such as the HP 4192A impedance analyzer. An example of performing PWAS E/M impedance spectroscopy is presented in Figure 3. The HP 4194A impedance analyzer (Figure 3(a)) reads the in situ E/M impedance of the PWAS attached to a specimen. It is applied by scanning a predetermined frequency range in the high kilohertz band (up to 15 MHz) and recording the complex impedance spectrum.

During a frequency sweep, the real part of the E/M impedance, $\text{Re}[Z(\omega)]$, follows the up and down variation as the structural impedance goes through the peaks and valleys of the structural resonances and anti-resonances (Figure 3(b)). By comparing the real part of the impedance spectra taken at various times during the service life of a structure, meaningful information can be extracted pertinent to structural degradation and ongoing damage development. On the other hand, analysis of the impedance spectrum supplies important information about the PWAS integrity. The frequency range used in the E/M impedance method must be high enough for the signal wavelength to be significantly smaller than the defect size. From this point of view, the high-frequency EMIS method differs from the low-frequency modal analysis approaches.

## PWAS EMIS modeling on composite

The first part of this section presents the MP-FEM model of a free PWAS in order to illustrate the EMIS calculation with the MP-FEM method. Then, we will describe how the MP-FEM modeling is used to study a PWAS mounted on a composite structure.

### *Free PWAS model*

A free PWAS has been modeled without the presence of the host structure in order to have a fundamental understanding of the multi-physics-based modeling approach and its efficiency using ANSYS multi-physics software with the implicit solver in the frequency domain. To perform the coupled-field analysis of PWAS transducers, we used coupled-field elements, which could deal with both mechanical and electrical fields. In the physics-based coupled-field analysis of piezoelectric materials, the stress field and the electric field are coupled to each other such that change in one field will induce change in the other field. The

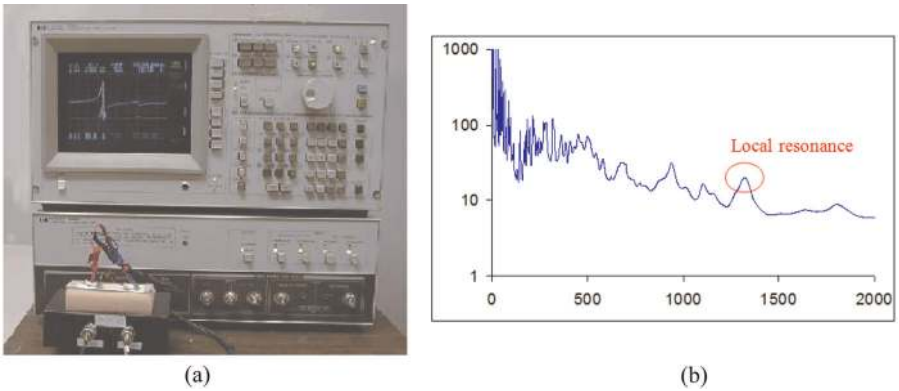


**Figure 3.** An example of measured impedance spectrum.

coupled-field finite elements used in our analysis are the brick elements (SOLID5, SOLID226) that have 8 or 20 nodes with up to six degrees of freedom (DOF) at each node. When used for piezoelectric analysis, an additional DOF, the electric voltage can be added in addition to the displacement DOF. Reaction forces FX, FY, and FZ correspond to the X, Y, and Z displacement DOF, respectively. The electrical charge $Q$ is the electrical reaction corresponding to the voltage DOF. The charge $Q$ is then used to calculate the admittance and impedance data. The admittance $Y$ is calculated as $I/V$, where $I$ is the current in ampere and $V$ is the applied potential voltage in volts. The current comes from the charge accumulated on the PWAS surface electrodes and is calculated as $I = j\omega \sum Q_i$, with $\omega$ being the operating frequency, $j$ is the complex number, and $\sum Q_i$ is the summed nodal charge. In this study, the PWAS was modeled using the three-dimensional (3D) MP-FEM approach with SOLID5 and SOLID226 elements. SOLID5 is a coupled-field brick with 8 nodes and up to six DOF per node, while SOLID226 has 20 nodes with up to four DOF per node. A free square-shaped PWAS of dimension $7 \times 7 \times 0.2\ \text{mm}^3$ was modeled. The APC-850 material properties were assigned to the PWAS as follows

$$C_p = \begin{bmatrix} 97 & 49 & 49 & 0 & 0 & 0 \\ 49 & 97 & 44 & 0 & 0 & 0 \\ 49 & 49 & 84 & 0 & 0 & 0 \\ 0 & 0 & 0 & 24 & 0 & 0 \\ 0 & 0 & 0 & 0 & 22 & 0 \\ 0 & 0 & 0 & 0 & 0 & 22 \end{bmatrix} \text{GPa} \quad (3)$$

$$[\varepsilon_p] = \begin{bmatrix} 947 & 0 & 0 \\ 0 & 605 & 0 \\ 0 & 0 & 947 \end{bmatrix} \times 10^{-8}\ \text{F/m} \quad (4)$$

$$[e_p] = \begin{bmatrix} 0 & 0 & 0 & 0 & 12.84 & 0 \\ 0 & 0 & 0 & 12.84 & 0 & 0 \\ -8.02 & -8.02 & 18.31 & 0 & 0 & 0 \end{bmatrix} \text{C/m}^2 \quad (5)$$

where $[C_p]$ is the stiffness matrix, $[\varepsilon_p]$ is the dielectric matrix, and $[e_p]$ is the piezoelectric matrix. The density of the PWAS material is assumed to be $\rho = 7600\ \text{kg/m}^3$.

Spectra from simulation and experiment of the free PWAS sweeping from 1 to 1000 kHz are presented in Figure 4. Globally, good matching is observed, but some differences are visible especially for the first resonance at ~250 kHz. Small differences are expected in the numerical response when compared to the experimental impedance because the wiring was not modeled and unavoidable and measuring errors may also occur. Nonetheless, this comparison illustrates that reasonable agreement can be obtained when MP-FEM method is used, which is an important improvement over the use of the conventional FEM method or the analytical models.

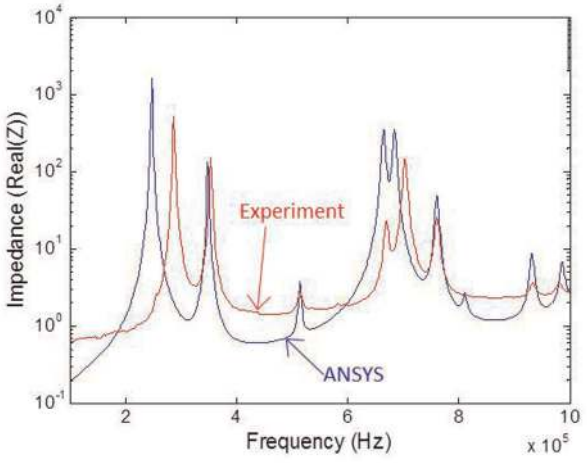


**Figure 4.** PWAS EMIS obtained from MP-FEM and measured from HP 4194 equipment, respectively.
PWAS: piezoelectric wafer active sensor; EMIS: electromechanical impedance spectroscopy; MP-FEM: multi-physics-based finite element method.

## PWAS EMIS model on orthotropic composite

In MP-FEM approach, the mechanical coupling between the structure and the sensor is implemented by specifying boundary conditions of the sensor, while the electromechanical coupling is modeled by multi-physics equations for the piezoelectric material. The first coupling allows the mechanical response sensed by the piezoelectric element to be reflected in its electric signature composite. The glass fiber reinforced polymer (GFRP) structure considered in this study is modeled as a homogeneous orthotropic material with assumed density $\rho = 1960\ \text{kg/m}^3$. The stiffness matrix C is estimated as

$$C = \begin{bmatrix} 28.7 & 5.7 & 3 & 0 & 0 & 0 \\ 5.7 & 28.7 & 3 & 0 & 0 & 0 \\ 3 & 3 & 12.6 & 0 & 0 & 0 \\ 0 & 0 & 0 & 4.1 & 0 & 0 \\ 0 & 0 & 0 & 0 & 4.9 & 0 \\ 0 & 0 & 0 & 0 & 0 & 4.9 \end{bmatrix} \text{GPa} \quad (6)$$

*Structural damping effects.* To simulate structural damping, stiffness-proportional or mass-proportional damping can be introduced in the frequency domain models of most FEM packages. This Rayleigh damping is defined as

$$[C] = \alpha_M [M] + \beta_K [K] \quad (7)$$

where $\alpha_M$ and $\beta_k$ are the mass- and stiffness-proportionality coefficients. The mass-proportional damping coefficient $\alpha_M$ introduces damping forces caused by the absolute velocities of the model and so simulates the idea of the model moving through a viscous "medium." The units of $\alpha_M$ are "1/time." The stiffness-proportional damping coefficient $\beta_k$ introduces damping proportional to the strain rate, which can be thought of as damping associated with the material itself. The units of $\beta_k$ are "time." In this study, the mass damping coefficients and the stiffness damping coefficients of the GFRP material were taken as $\alpha = 0.2$ and $\beta = 10^{-8}$, respectively.[15] With the application of this principle, the coupled-field FEM matrix element can be expressed as follows[16,17]

$$\begin{bmatrix} [M] & [0] \\ [0] & [0] \end{bmatrix} \begin{Bmatrix} \{\ddot{u}\} \\ \{\ddot{V}\} \end{Bmatrix} + \begin{bmatrix} [C] & [0] \\ [0] & [0] \end{bmatrix} \begin{Bmatrix} \{\dot{u}\} \\ \{\dot{V}\} \end{Bmatrix} + \begin{bmatrix} [K] & [K^Z] \\ [K^Z]^T & [K^d] \end{bmatrix} \begin{Bmatrix} \{u\} \\ \{V\} \end{Bmatrix} = \begin{Bmatrix} \{F\} \\ \{L\} \end{Bmatrix} \quad (8)$$

where $[M]$, $[C]$, and $[K]$ are the structural mass, damping, and stiffness matrices, respectively; $\{u\}$ and $\{V\}$ are the vectors of nodal displacement and electric potential, respectively, with the dot above variables denoting time derivative; $\{F\}$ is the force vector; $\{L\}$ is the vector of nodal, surface, and body charges; $\{K^Z\}$ is the piezoelectric coupling matrix; and $[K^d]$ is the dielectric conductivity.

This formulation is very convenient for evaluating the admittance signatures as it is measured by the impedance analyzer in the EMIS technique. The complex admittance signature, which is the ratio of electric current to voltage, can be expressed as $\bar{Y} = \bar{I}/\bar{V}$, with $\bar{V}$ as the voltage applied by the impedance analyzer (1 V in our case) and $\bar{I}$ as the modulated current, with the bars above the variables indicating complex terms.

The GFRP composite beam specimen dimensions are 60 × 1 mm$^2$ and the PWAS 7 × 0.2 mm$^2$. For a plane-strain analysis, only a longitudinal section of the specimen and PWAS need be analyzed; hence, a two-dimensional (2D)-meshed MP-FEM model can be used, which reduces considerably the computational time. The 2D plane element PLANE82 is used for the GFRP beam; this element has eight nodes and three DOF at each node. The 2D plane element PLANE223 is used to model the PWAS using the coupled-field formulation presented in the section "PWAS EMIS model on orthotropic composite." Then, the impedance spectrum up to 1 MHz was calculated.

Figure 5 shows the comparison of the real part of the impedance against the frequency, with and without the structural damping. It can be seen that addition of damping increases the off-resonance base of the spectrum while decreasing the resonance peaks. This attenuation increases with frequency as illustrated by the difference observed in high-frequency range above 600 kHz. Based on the initial investigation, we adjusted the damping coefficients assumed in the rest of this study to match actual measurements.

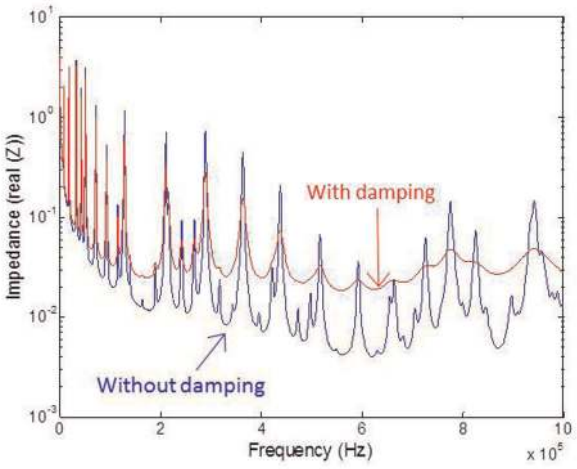


**Figure 5.** Damping effect in the PWAS–orthotropic composite structure interaction model.
PWAS: piezoelectric wafer active sensor.

*Bonding adhesive layer effects.* For PWAS–structure interaction, the mechanical deformation of the PWAS transducer is transferred to the host structure through the bonding adhesive layer. The transferred shear force has been found to correlate with the bonding layer thickness.[1] In our study, a 30-μm thick isotropic bonding layer is considered. The density, Young's modulus, and Poisson ratio of the bonding layer were taken as $\rho = 1700\,\text{kg/m}^3$, $E = 5$ GPa, and $\nu = 0.4$ as recommended by Ong et al.[18] Two models are developed and compared. The first model has the PWAS directly connected to the structure without adhesive, while the second model incorporates the bonding layer as a third sub-structure. The resulting impedance spectra are given in Figure 6. It is apparent that the effect of the bonding layer becomes more important as the frequency increases; for lower frequencies, the effect of adding the bonding layer is hardly perceptible.

*PWAS self-diagnosis: bonding degradation.* Park et al.[19] presented a sensor diagnosis and validation process that performs in situ monitoring of the operational status of PWASs installed on isotropic metallic structures without damping. It was found that the sensor–structure bonding defects can modify the measured admittance and impedance spectra. We modeled this situation with

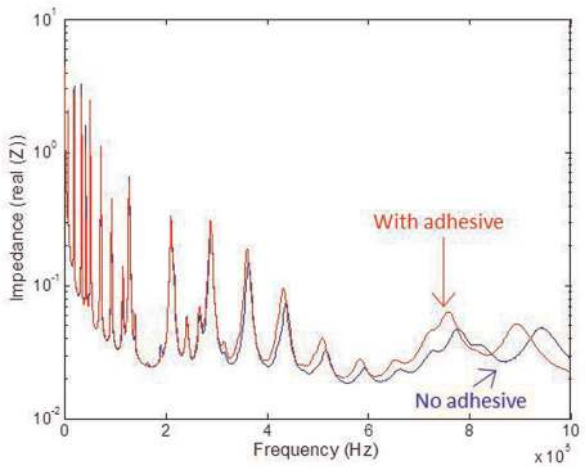


**Figure 6.** MP-FEM predicted impedance spectra of a PWAS attached to a structure with and without an adhesive bonding layer.
PWAS: piezoelectric wafer active sensor; MP-FEM: multi-physics-based finite element method.

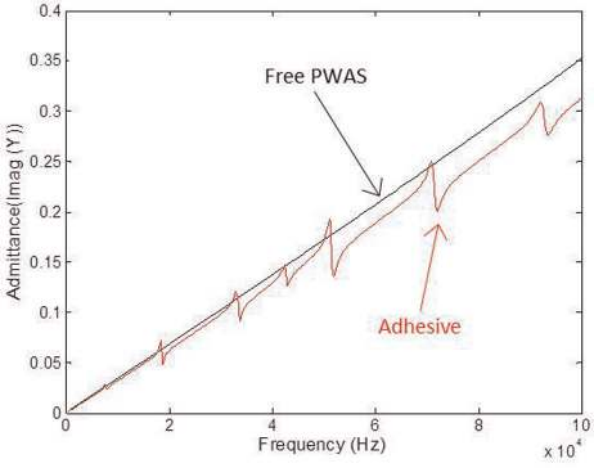


**Figure 7.** MP-FEM prediction of the admittance (imaginary part) of a free PWAS compared with that of a PWAS adhesively bonded to a structure.
PWAS: piezoelectric wafer active sensor; MP-FEM: multi-physics-based finite element method.

the MP-FEM method as shown in Figure 7. It is seen that the PWAS admittance moves upward when the physical situation changes from bonded condition to free condition. In reality, when PWAS disbonds from an undamped isotropic structure, its behavior will resemble that of the free PWAS, that is, its admittance will display the imaginary part of its spectrum as moving upward and a disappearance of the structural resonance peaks as reported in Ref. [19]. This method offers a useful means to monitor sensor installation of isotropic undamped metallic structure.


**Figure 8.** Bonding degradation model.
PWAS: piezoelectric wafer active sensor; GFRP: glass fiber reinforced polymer.

We continued this simulation study of the PWAS bond degradation by removing the adhesive material starting at one edge of the PWAS as shown in Figure 8. Several situations were modeled: (a) free PWAS, (b) perfect bonding (0% adhesive degradation), (c) 14% degradation (14% of the length of the adhesive layer removed), and (d) 42% degradation (42% of the length of the adhesive layer removed).

The resulting admittance spectra (the imaginary part) are shown in Figure 9(a). It is clear that the bonding degradation results in a downward shift in the slope of the imaginary parts of the admittance. The impedance spectra have also been studied to understand the effect of bonding degradation. Figure 9(a) shows the imaginary part of the admittance spectrum for frequencies up to 100 kHz. It is apparent that, as the bond degrades, the zigzags indicative of structural resonances diminish more and more until they can no longer be sensed when the PWAS is completely disbanded from the structure (free PWAS).

However, the rule of upward shift reported in Ref. [19] does not seem to apply for partial disbanding, because the shifts of the imaginary impedance curves are initially downward and then finally upward. Figure 9(b) shows the change in the real part of the impedance spectrum in the range up to 1 MHz. We notice that, as the adhesive layer between the PWAS and the structure degrades the baseline of the spectrum and hence the structural resonances peaks mode up. On the higher frequency range above 600 kHz, a frequency shift to the left is clearly observed when the degradation of the adhesive layer increases. Finally, when the PWAS is completely disbanded, the resonances of the free PWAS are fully recovered.

*PWAS self-diagnosis sensor damage.* The sensor damage can be modeled as material loss by cutting off parts of the PWAS edge (Figure 10). In this study, a 1-mm length loss was considered.

The resulting admittance spectrum (imaginary part) is shown in Figure 11(a). It is clear that the bonding degradation results in a downward shift in the slope of the imaginary parts of the admittance. This observation is consistent with the analytical results obtained by

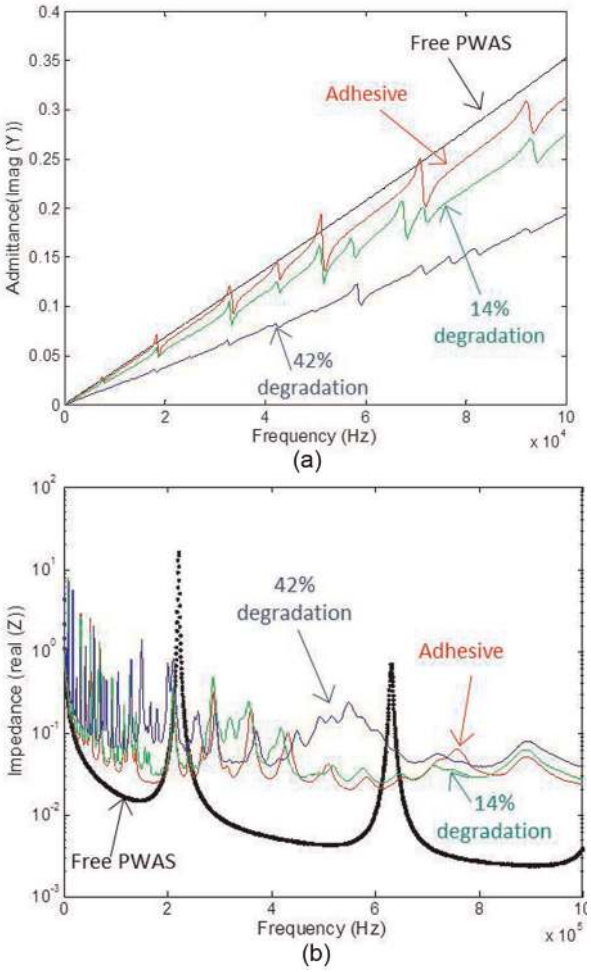


**Figure 9.** Bonding degradation: (a) observed in the imaginary part of the admittance spectrum for frequencies up to 100 kHz; (b) observed in the real part of the impedance spectrum for frequencies up to 1 MHz.
PWAS: piezoelectric wafer active sensor.

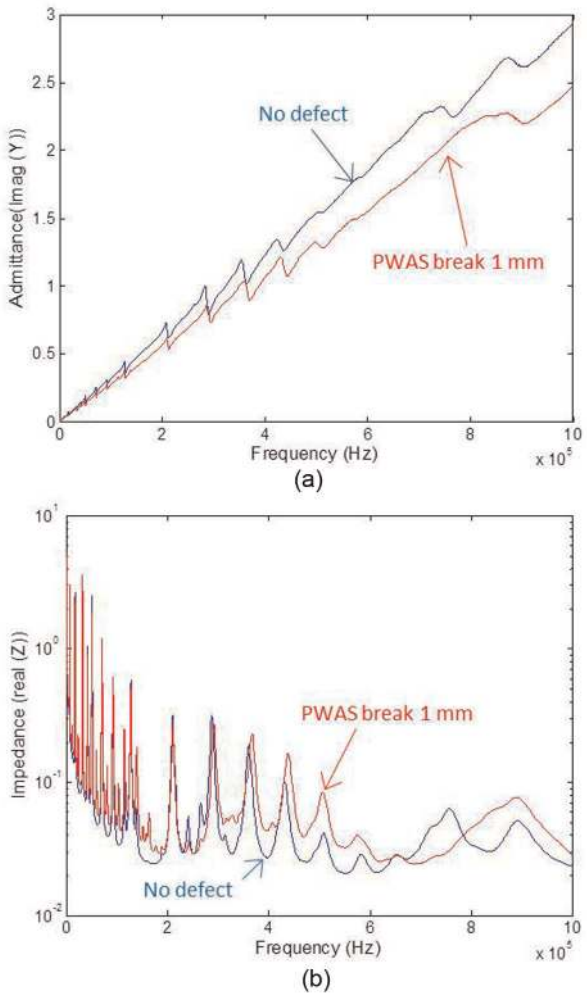


**Figure 11.** Sensor degradation: (a) observed admittance spectra; (b) observed impedance spectra.
PWAS: piezoelectric wafer active sensor.

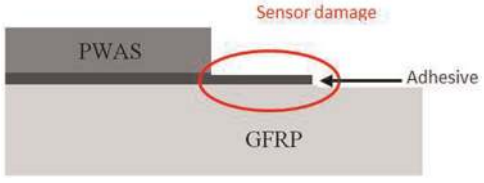


**Figure 10.** Sensor breakage model.
PWAS: piezoelectric wafer active sensor; GFRP: glass fiber reinforced polymer.

Park et al.,[19] for an undamped isotropic metallic structure.

The effect of PWAS degradation on the impedance spectra is shown in Figure 11(b). We notice that the baseline of the impedance curve moves up when the adhesive sensor degrades (as was also previously observed for the case of adhesive degradation). However, the sensing of the structural resonances seems to be unaffected at the lower end of the spectrum. At the higher end of the spectrum, a frequency shift toward higher values is observed when the PWAS is degraded.

It is apparent from this study that the imaginary part of the admittance reading and the real part of the impedance can serve as a useful way to detect bonding layer and sensor degradation, respectively.

## *Modeling of the PWAS EMIS structural damage detection*

In the modeling of the structural damage detection, the damage was modeled as material properties changed.

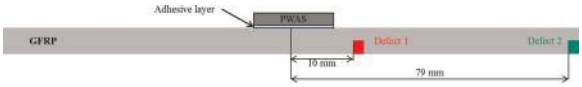


**Figure 12.** PWAS EMIS defect–detection model.
PWAS: piezoelectric wafer active sensor; EMIS: electromechanical impedance spectroscopy; GFRP: glass fiber reinforced polymer.

Damage was modeled at scale of a single element ($500 \times 500\ \mu m^2$) by decreasing the Young's modulus, $E$, by 5%, 10%, 15%, and 20%, respectively. Two situations were studied: one with the damage defect located at 10 mm away from the PWAS center line (Figure 12) and the other located 79 mm away. Impedance spectra for "no defect," "defect at location 1" (10 mm), and "defect at location 2" (79 mm) were calculated with the MP-FEM method in five frequency bands: 0–200, 200–400, 400–600, 600–800, and 800–1000 kHz. These spectra were studied and analyzed using a "damage index" (DI) approach.

The DI was calculated as a change with respect to a baseline state. To evaluate the DI, we use the root mean square deviation (RMSD) defined as

$$\mathrm{RMSD} = \sqrt{\frac{\sum_N [\mathrm{Re}(Z_i) - \mathrm{Re}(Z_i^0)]^2}{\sum_N [\mathrm{Re}(Z_i^0)]^2}} \tag{9}$$

where $Z_i$ represents the $i$th element in the measurement spectrum, $Z_i^0$ represents the $i$th element in the baseline, and $N$ is the data length.

The DI curves for defect at location 1 calculated in five different frequency bands are presented in Figure 13(a), whereas the curves for defect at location 2 are presented in Figure 13(b). It can be seen that the PWAS EMIS can pick up the difference between no defect and a defect of small scale and far away from the sensor location, although the difference is much smaller for the defect that is further away. Also noticed is that different frequency bands have different sensitivity to the defect presence, with the 200–400 kHz band being the most sensitive one in our case.

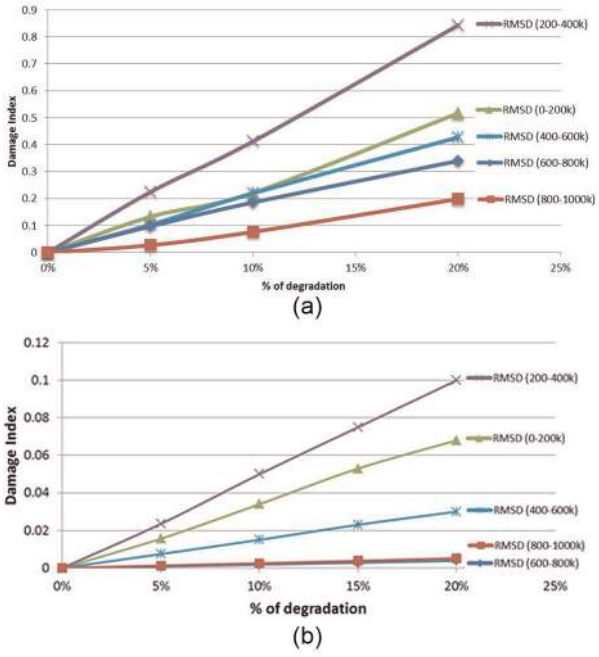


**Figure 13.** Defect detection with PWAS EMIS method: (a) DI curves for defect at location 1 (10 mm from PWAS); (b) DI curves for defect at location 2 (79 mm from PWAS).
DI: damage index; PWAS: piezoelectric wafer active sensor; EMIS: electromechanical impedance spectroscopy; RMSD: root mean square deviation.

## PWAS EMIS delamination detection modeling

In this part of our study, we modeled an actual five-layer-laminated GFRP specimen. We also studied the effect of a delamination introduced between the layers 3 and 4 as illustrated in Figure 14. The delamination is simulated by disengaging (i.e. not being glued together) the elements from the bottom part of the designated area 7 (A7) and the elements from the top part of the designated area 4 (A4). When the model is meshed, double nodes will occur at the same coordinates of the interfacial lines (represented by a red line in Figure 14). The delamination is simulated with three different lengths: 0.1, 0.5, and 1 mm. The total length of the GFRP specimen was 60 mm, hence, these delaminations represented 0.167%, 0.833%, and 1.67%, respectively. In each case, five frequency bands were considered: 0–200, 200–400, 400–600, 600–800, and 800–1000 kHz. The data were then analyzed with the DI method described in the previous section.

The resulting DI curves presented in Figure 15 reflect the impedance changes caused by a delamination increasing in step up to a length of 1 mm. The 0.5 mm delamination, representing less than 1% of the beam length, was clearly detected by an increase in the DI curve. It is seen that both the higher frequency range

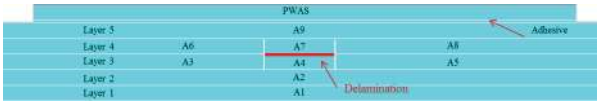


**Figure 14.** PWAS EMIS delamination detection model.
PWAS: piezoelectric wafer active sensor; EMIS: electromechanical impedance spectroscopy.

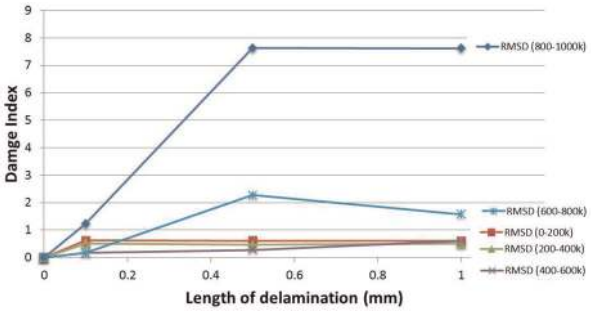


**Figure 15.** DI curves for delamination detection with PWAS EMIS method.
DI: damage index; PWAS: piezoelectric wafer active sensor; EMIS: electromechanical impedance spectroscopy; RMSD: root mean square deviation.

(800–1000 kHz) and the medium–high range (600–800 kHz) are more sensitive to detect the small delamination considered in this simulation. This is to be expected because the higher frequencies are more sensitive to the detection of small defects such as the delamination considered in this laminated composite specimen.

Knowing that a delamination defect is very dangerous in composite materials because the defect strongly degrades the compressive and buckling strength, it seems very encouraging to report that the detection of very small delaminations can be made with the EMIS method applied at very high frequency (MHz range).

## 3D modeling and experimental validation

A five-layer woven GFRP specimen of 60 mm length, 10 mm width, and 1 mm thickness has been instrumented with a round PWAS of 7 mm diameter and 0.2 mm thickness in the middle. The impedance spectrum is first obtained experimentally using the HP 4192A impedance analyzer in the frequency range 10 kHz to 15 MHz for later comparison with the result from MP-FEM model.

### *3D MP-FEM model*

The test specimen is numerically modeled with the MP-FEM method using a 3D mesh as illustrated in Figure 16. The SOLID186 (3D 20-node) layered structural solid element is used to model the five-layer-laminated GFRP composite specimen with layer orientation of 0° on the $x$-axis; the adhesive layer is modeled with the SOLID95 (3D 20-node) element. The PWAS transducer is modeled with the SOLID226 (3D 20-node coupled-field) element. Each element has 20 nodes.

For low frequency (below 500 kHz), medium frequency (500 kHz–5 MHz) and high frequency (5–15 MHz), the size of the mesh is 1, 0.5, and 0.1 mm, respectively, to obtain a good convergence of the problem.

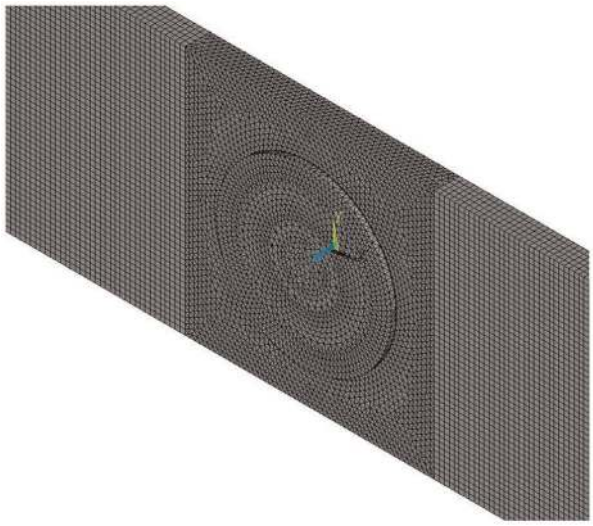

**Figure 16.** 3D model of the GFRP, the adhesive, and the PWAS.
3D: three-dimensional; PWAS: piezoelectric wafer active sensor; GFRP: glass fiber reinforced polymer.

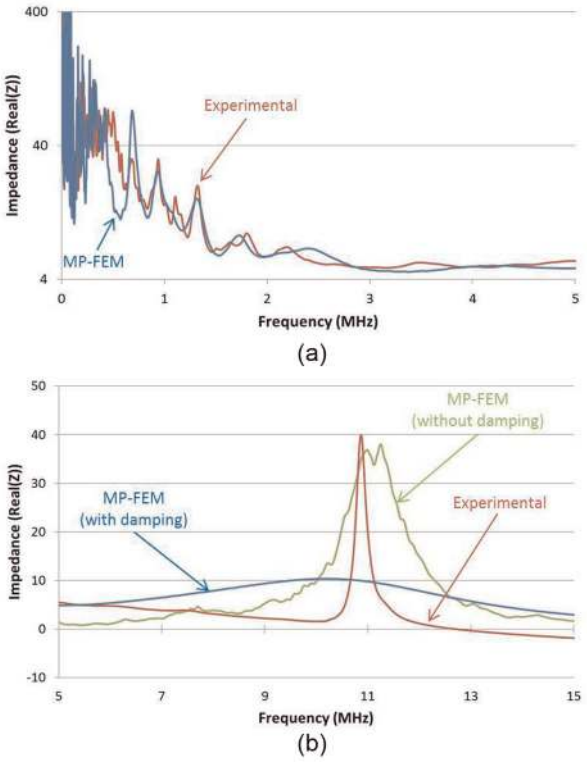


**Figure 17.** Comparison of experimental and 3D MP-FEM model impedances spectra of laminate GFRP: (a) for a frequency range 10 kHz–5 MHz; (b) for a frequency range 5–15 MHz.
MP-FEM: multi-physics-based finite element method; GFRP: glass fiber reinforced polymer.

The impedance spectra together with the experimental result are presented in Figure 17. In Figure 17(a), the results are in the range up to 5 MHz. It is apparent that a good agreement between the experiments and 3D MP-FEM simulation has been achieved. The good matching is achieved by adjusting the damping coefficients used in the structural model. The correlation of the modal frequencies between the experimental and the numerical results is quite good, especially at higher frequencies. However, some discrepancies in the magnitudes of some resonances are observed, especially in the range of 450–650 kHz. It is interesting to see that the best match is obtained in the 700 kHz to 2 MHz frequency range. This is very beneficial, because this frequency range has shown the best early detection of delamination damage in the previous section.

It seems that at high frequency (5–15 MHz), the vibration is very localized and so the bonding condition and the geometry of the PWAS is very important. In our simulation, the bonding layer and the PWAS geometry were assumed perfect. In reality, this is not true and this may explain the larger difference between the experimental and the simulation results at high frequency. Moreover, the magnitude of the resonance peak at high frequency is very small due to high-frequency damping effect, which is nonlinear and hence hard to simulate with our linear approach.

Figure 17(b) shows a comparison of the impedance spectra in a very high-frequency range (5–15 MHz). Only one peak is observed at ˜11 MHz; this peak corresponds to the thickness mode resonance of the PWAS transducer.

The comparison between the 3D simulation and experimental results has revealed two different regions of behavior: (1) below 5 MHz, the experimental result matches the result from a 3D model with structural damping (Figure 17(a)) and (2) above 7 MHz, the experimental result matches better with a 3D model without structural damping (Figure 17(b)). One possible explanation is that at lower frequency the vibration covers a larger area and the overall structural damping is important, whereas at high frequency the vibration is localized in thickness mode resulting that the structural damping has negligible effect.

In comparison with other models of the EMIS technique, the model discussed here exhibits remarkable robustness at very high frequency.

For instance, most of the models studied by other researchers,[9,18,20–22] either analytical or semi-analytical (FEM plus mechanical coupling with the PWAS), showed good results only for lower frequencies, that is, below 100 kHz. These shortcomings of the previous study may be attributed to a number of reasons. First, it should be noted that the actual interaction between the PWAS transducer and the host structure through the bonding layer involves a finite area of the size of the bonded area. Simplification of the interaction in this finite area and reduction to point forces or moments would render some vibrational modes unexcitable, as well as giving an inaccurate prediction of certain high frequencies. Second, the basic assumption of neglecting the effect of bonding layer adopted by the other researcher is not realistic at high frequency. Some researchers[8,9,18] have introduced a modification to the E/M impedance coupling equation by incorporating the effect of bonding. However, this was not always sufficient to achieve a good agreement with the experimental data especially at high frequency.

Moreover, the damping effect for the low frequency and the high frequency is important to understand the interaction between the host structure and the PWAS. So at low frequency, the damping effect of the composite specimen is very important, because the vibration given by the PWAS is global and covers the complete structure, whereas at high frequency the structural vibration is localized near the PWAS.

### *Damping coefficient effect*

After considering these interesting remarks on the damping effect at low and high frequencies, it is useful to better understand the physical phenomena of the damping effect. First, the damping effect depends on two parameters:

1. The mass-proportional damping coefficient $\alpha_M$ introduces damping forces caused by the absolute velocities of the model and so simulates the idea of the model moving through a viscous "medium";
2. The stiffness-proportional damping coefficient $\beta_k$ introduces damping proportional to the strain rate, which can be thought of as damping associated with the material itself.

It is therefore legitimate to ask what is the most important damping coefficient at low and high frequencies.

The experimental and 3D modeling results at high-frequency range (10–1000 kHz) are presented in Figure 18. This figure shows the impedance spectra with the variation of the mass-proportional damping coefficient $\alpha_M$. It is apparent that we observe no variation of the impedance spectra with the variation of $\alpha_M$. In other words, the damping effect of the impedance spectra is not due to the mass-proportional coefficient $\alpha_M$ but only due to the stiffness-proportional coefficient $\beta_k$.

The experimental and 3D modeling results in a very high-frequency range (7–15 MHz) are presented in Figure 19. Figure 19(a) shows the impedance spectra

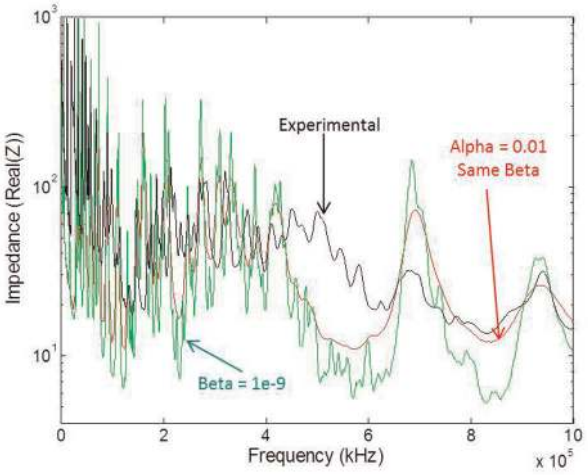


**Figure 18.** Comparison of experimental and modeled (damping variation) impedances of GFRP for a frequency range 10 kHz–1 MHz.
GFRP: glass fiber reinforced polymer.

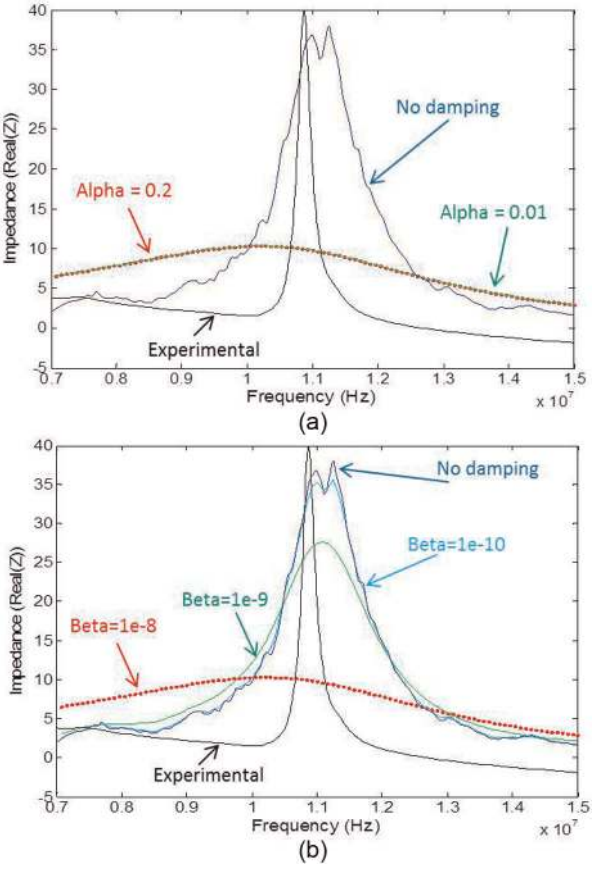


**Figure 19.** Comparison of experimental and modeled impedances of GFRP for a frequency range 7–15 MHz: (a) effect of the mass-proportional damping coefficient $\alpha_m$; (b) effect of the stiffness-proportional damping coefficient $\beta_k$.
GFRP: glass fiber reinforced polymer.

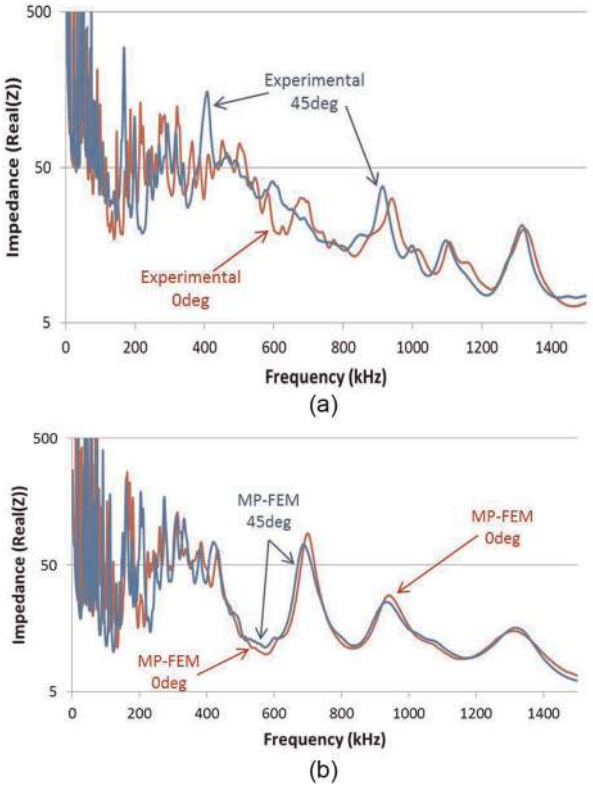


**Figure 20.** Fiber orientation effect on the impedance spectra in high frequency (10–1500 kHz): (a) experimental results for 0° and 45° in the *x*-axis; (b) MP-FEM results for 0° and 45° in the *x*-axis.

with the variation of the mass-proportional damping coefficient $\alpha_M$. It is apparent that we observe no variation of the impedance spectra with the variation of $\alpha_M$. In other words, the damping effect of the impedance spectra is not due to the mass-proportional coefficient $\alpha_M$ but only due to the stiffness-proportional coefficient $\beta_k$, as showed in Figure 19(b). Indeed, when decreases, that is, the damping is reduced, the curve looks like the curve without damping.

In summary, the Rayleigh damping can be defined for the frequency below 5 MHz as follows

$$[C] = \beta_K[K] \tag{10}$$

where $\beta_K$ is the stiffness-proportionality coefficient. And the Rayleigh damping can be defined for the frequency above 5 MHz as $[C] = 0$.

## *Fiber orientation effect*

For laminate composite material, the fiber orientation is very important for the mechanical behavior of the structure. So we decided to study the EMIS for

different fiber's orientation to know if the impedance spectra change with different orientation.

The experimental results for two different fiber orientations (0° and 45°) in a high-frequency range (10 kHz to 5 MHz) are presented in Figure 20(a). It is apparent that a frequency shift to the lower frequency is present for the fiber orientation of 45°. Figure 20(b) shows the MP-FEM impedance spectra for these two different orientations. It is apparent that a frequency shift to the lower frequency is present for the layer orientation of 45°; this is in agreement with the experimental results.

## Conclusion

This article has presented a numerical and experimental study on the use of PWASs to detect damage in GFRP structures using the EMIS method. The MP-FEM was used to simulate the electromechanical impedance by the direct application of electric voltage to the PWAS and measurement of the resulting electric current. The EMIS of a free PWAS revealed its own resonance very well; a very good agreement was obtained between the measured and predicted impedance and admittance curves. Then, a PWAS bonded on a GFRP specimen was modeled with the 2D and then with the 3D MP-FEM approach. The 2D MP-FEM was used to understand the sensor–structure interaction under various damage scenarios. The effect of bonding layer degradation and sensor degradation on the EMIS spectrum was studied. It is found that the bonding layer degradation and the sensor degradation can be assessed by monitoring the real part of the impedance and the imaginary part of the admittance. The structural damage was next modeled by changing the Young's modulus in a small region of the specimen. Such localized damage was simulated both near (10 mm) and far (79 mm) from the PWAS transducer. It was found that both near-field (10 mm) and medium-far (79 mm) damages can be detected using a RMSD DI, but the detection in near field is stronger than in the far field. Next, the detection of delaminations of various sizes was investigated. It was found that the high-frequencies ranges (800–1000 and 600–800 kHz) are more susceptible to delamination detection, while low frequencies are more sensitive to changes in the Young modulus.

The 3D MP-FEM method was used to simulate realistic situations that were then compared with EMIS experimental results. The 3D MP-FEM model gave excellent reproduction of the measured EMIS results; however, the required computation is orders magnitude larger than the 2D MP-FEM. It was found that this numerical model exhibited remarkable robustness at a very high frequency. We also found that the structural damping is very important for proper modeling of the interaction between the host structure and the PWAS. However, its effect at lower frequencies (<5 MHz) is different from its effect at higher frequencies (>7 MHz). At lower frequencies, the damping effect of the composite specimen is very important, because the vibration given by the PWAS has a global coverage over the whole structure; in contrast, at higher frequencies, the vibration in the structure is more localized near the PWAS and the structural damping does not play a good role.

Future study should continue the 3D MP-FEM investigation in the effect of different fiber orientation and the effect of different types of defects (cracks, fiber break, delamination, etc.) and comparison of these findings with the 2D MP-FEM results as well as with experimental results consisting of EMIS readings on specimens with internal damage and PWAS disbonds or damage.

### Funding

This study was performed under the support of the Air Force Office of Scientific Research FA9550-09-1, Program Director Dr David Stargel.

### References

1. Giurgiutiu V. *Structural health monitoring with piezoelectric wafer active sensors*. Elsevier Academic Press, 2008. ISBN 978-0120887606.
2. Makkonen T, Holappa A, Ellä J, et al. Finite element simulations of thin-film composite BAW resonators. *IEEE Trans Ultrason Ferroelectr Freq Control* 2001; 48: 1241–1258.
3. Lalande F. *Modelling of the induced strain actuation of shell structures*. Blacksburg, VA: Virginia Polytechnic Institute and State University, 1995.
4. Lim YY, Bhalla S and Soh CK. Structural identification and damage diagnosis using self-sensing piezo-impedance transducers. *Smart Mater Struct* 2006; 15(4): 987–995.
5. Liu W and Giurgiutiu V. Finite element simulation of piezoelectric wafer active sensors for structural health monitoring with coupled field elements. In: *6th International Workshop on Structural Health Monitoring*, Stanford, CA, 2007.
6. Naidu ASK and Soh CK. Damage severity and propagation characterization with admittance signatures of piezo transducers. *Smart Mater Struct* 2004; 13(2): 393.
7. Crawley EF and Anderson EH. Detailed models of piezoceramic actuation of beams. *J Intel Mat Syst Str* 1990; 3: 166–185.
8. Liang C, Sun FP, and Rogers CA. Coupled electromechanical analysis of adaptive material systems – determination of the actuator power consumption and system energy transfer. *J Intel Mat Syst Str* 1994; 5(1): 12–20.

9. Bhalla S. *A mechanical impedance approach for structural identification, health monitoring and non-destructive evaluation using piezo-impedance transducers*. Singapore: Nanyang Technological University, 2004.
10. Bois C, Herzog P and Hochard C. Monitoring of delamination in laminated composite beam using in-situ measurments and parametric identification. *J Sound Vib* 2007; 299: 786–805.
11. Bois C and Hochard C. Monitoring of laminated composites delamination based on electromechanical impedance measurement. *J Intel Mat Syst Str* 2004; 15: 59–67.
12. Chaudhry Z, Joseph T, Sun FP, et al. Local-area health monitoring of aircraft via piezoelectric actuator/sensor patches. In: *Smart structures and integrated systems (Proceedings of SPIE)*. San Diego, CA: 1995, pp. 268–276.
13. Park G, Cudney HH and Inman DJ. Impedance-based health monitoring of civil structural components. *J Infrastruct Syst* 2000; 6(4): 153–160.
14. Park G, Sohn H, Farrar CR, et al. Overview of piezoelectric impedance-based health monitoring and path forward. *Shock Vib Digest* 2003; 35(6): 451–463.
15. Gresil M. *Contribution to the study of a health monitoring associated with an electromagnetic shielding for composite materials*. Dissertation Thesis, Ecole Normale Superieure de Cachan, 2009, 241 pp.
16. Moveni S. *Finite element analysis, theory application with ANSYS*. Upper Saddle River, NJ: Pearson Education, 2003.
17. ANSYS. *ANSYS reference manual, R. 8.1*. Canonsburg, PA: ANSYS, 2004.
18. Ong CW, Yang Y, Wong YT, et al. The effects of adhesive on the electro-mechanical response of a piezoceramic transducer coupled smart system. *P SPIE*, 2002; 5062: 241–247.
19. Park G, Farrar CR, Lanza Di Scalea F, et al. Performance assessment and validation of piezoelectric active-sensors in structural health monitoring. *Smart Mater Struct* 2006; 15(6): 1673–1683.
20. Zagrai A and Giurgiutiu V. Electro-mechanical impedance method for crack detection in thin plates. *J Intel Mat Syst Str* 2001; 12: 709–718.
21. Giurgiutiu V and Zagrai A. Damage detection in simulated aging-aircraft panels using the electro-mechanical impedance technique. In: *Adaptive structures and material systems symposium, ASME winter annual meeting*, Orlando, FL, 2000.
22. Lim YY. *Structural identification by smart materials*. Singapore: Nanyang Technological University; 2004.